Traceable size determination of nanoparticles, a comparison among European metrology institutes

2012 Meas. Sci. Technol. 23 125005

(http://iopscience.iop.org/0957-0233/23/12/125005)

IOP PUBLISHING MEASUREMENT SCIENCE AND TECHNOLOGY

Meas. Sci. Technol. **23** (2012) 125005 (15pp) doi:10.1088/0957-0233/23/12/125005

Traceable size determination of nanoparticles, a comparison among European metrology institutes

Felix Meli[1,8], **Tobias Klein**[2], **Egbert Buhr**[2], **Carl Georg Frase**[2],
Gudrun Gleber[3], **Michael Krumrey**[3], **Alexandru Duta**[4], **Steluta Duta**[4],
Virpi Korpelainen[5], **Roberto Bellotti**[6], **Gian Bartolo Picotto**[6],
Robert D Boyd[7] **and Alexandre Cuenat**[7]

[1] Swiss Federal Office of Metrology (METAS), Lindenweg 50, 3084 Wabern, Switzerland
[2] Physikalisch-Technische Bundesanstalt (PTB), Bundesallee 100, D-38116 Braunschweig, Germany
[3] Physikalisch-Technische Bundesanstalt (PTB), Abbestr. 2-12, D-10587 Berlin, Germany
[4] National Institute of Metrology (INM), Sos. Vitan-Bârzesti 11, 042 122 Bucharest, Romania
[5] Centre for Metrology and Accreditation (MIKES), PO Box 9, FI-02151 Espoo, Finland
[6] Istituto Nazionale di Ricerca Metrologica (INRIM), Stradadelle Cacce 73, I-10135 Torino, Italy
[7] National Physical Laboratory (NPL), Teddington, Middlesex, TW11 0LW, UK

E-mail: felix.meli@metas.ch

Received 23 December 2011, in final form 15 October 2012
Published 20 November 2012
Online at stacks.iop.org/MST/23/125005

Abstract
Within the European iMERA-Plus project 'Traceable Characterisation of Nanoparticles' various particle measurement procedures were developed and finally a measurement comparison for particle size was carried out among seven laboratories across six national metrology institutes. Seven high quality particle samples made from three different materials and having nominal sizes in the range from 10 to 200 nm were used. The participants applied five fundamentally different measurement methods, atomic force microscopy, dynamic light scattering (DLS), small-angle x-ray scattering, scanning electron microscopy and scanning electron microscopy in transmission mode, and provided a total of 48 independent, traceable results. The comparison reference values were determined as weighted means based on the estimated measurement uncertainties of the participants. The comparison reference values have combined standard uncertainties smaller than 1.4 nm for particles with sizes up to 100 nm. All methods, except DLS, provided consistent results.

Keywords: nanoparticles, gold colloids, traceable measurement, calibration, comparison

(Some figures may appear in colour only in the online journal)

1. Introduction

Particle size measurements have a direct impact on the reliability of nanoparticle-based products and provide the essential underpinning metrology for toxicological studies of nanoparticles and nanotubes. Nanoparticles have unique properties that can be exploited commercially, for example as highly concentrated suspensions in the ink industry, as drug delivery agents for the pharmaceutical industry or in novel advanced composite materials in the transport industries. The roadmap on dimensional metrology for micro- and nano-technologies produced by the European Association of National Metrology Institutes (EURAMET) has put nanoparticle size distribution metrology on top of its priorities [1, 2].

Particle sizing instruments are based on different physical principles such as light diffraction, particle transport properties in various media or by directly accessing the size from

---

[8] Author to whom any correspondence should be addressed.

Table 1. Participants and applied methods.

Participant	Acronym	Method
Physikalisch-Technische Bundesanstalt, Berlin, Germany	PTB	SAXS
Physikalisch-Technische Bundesanstalt, Braunschweig, Germany	PTB	TSEM
National Institute of Metrology, Bucharest, Romania	INM	SEM
Swiss Federal Office of Metrology, Wabern, Switzerland	METAS	AFM
Centre for Metrology and Accreditation, Espoo, Finland	MIKES	AFM
Istituto Nazionale di Ricerca Metrologica, Torino, Italy	INRIM	AFM
National Physical Laboratory, Teddington, UK	NPL	DLS

Table 2. Product, material and nominal size of the samples used in this comparison.

Product	Material	Nominal size	Supplier	Reference
NIST RM 8011	Colloidal gold	10 nm	NIST	[9]
NIST RM 8012	Colloidal gold	30 nm	NIST	[9]
NIST RM 8013	Colloidal gold	60 nm	NIST	[9]
IRMM-304	Colloidal silica	40 nm	IRMM	[10]
Duke 3050A	Polystyrene	50 nm	Duke (Thermo Scientific)	[11]
Duke 3100A	Polystyrene	100 nm	Duke (Thermo Scientific)	[11]
Duke 3200A	Polystyrene	200 nm	Duke (Thermo Scientific)	[11]

microscope images. Depending on the applied principles the traceability to the definition of the SI unit 'metre' can be very complex. Additionally, there are differences in the acquired measurands, i.e. the single particle diameter definition and the method used for the mean value calculation. In many cases the easiest way to obtain validated and traceable results is to use certified particle reference materials, preferably reference particle samples that are calibrated at national metrology institutes (NMIs) providing a verifiable link to the relevant SI unit.

The EURAMET iMERA-Plus project 'Traceable Characterisation of Nanoparticles' developed methods required for traceable calibration of nanoparticle sizes at NMIs. Comparison measurements were carried out in order to validate the methods and the uncertainty estimations developed at six NMIs (table 1).

While consistent independent measurements have been demonstrated for NIST SRM 1963, a 100 nm latex reference material [3–6], so far only a few interlaboratory comparisons of nanoparticles have been carried out and considerable differences were discovered especially between the different methods [7, 8]. A detailed interpretation of these preliminary studies is quite difficult because the participants did not provide measurement uncertainties or their traceability routes. In principle, some of the laboratories could have used the same reference material to calibrate their instruments and therefore provided correlated results, possibly even including systematic deviations.

The comparison presented here required the methods applied by the NMIs to be independently traceable to realizations of the SI unit 'metre'. The traceability should be provided within the participants' institute (in-house) and the applied methods should not rely on third party particle size standards which were calibrated elsewhere. The methods applied within this comparison were atomic force microscopy (AFM), dynamic light scattering (DLS), small-angle x-ray scattering (SAXS), scanning electron microscopy (SEM) and scanning electron microscopy in transmission mode (TSEM), see table 1.

Figure 1. Distributed set of seven particle samples.

2. Particle samples and organization

Based on the outcome of a survey among the participants which gathered information on particle sources and measurement conditions, a set of seven liquid suspensions containing high quality particles was selected. The chosen particles were made from polystyrene, silica and gold with a size range from 10 to 200 nm (figure 1, table 2). The liquid suspensions were all water based including additives to avoid coagulation. Possible additives mentioned by the suppliers were tetrasodium pyrophosphate for polystyrene, sodium hydroxide (NaOH) for silica and citrate for the gold colloids. The samples were made by three different producers. All samples procured were requested to belong to the same batch. METAS repacked the polystyrene samples in order to send a complete set to each partner, including all available documentation. The sources were NIST, Gaithersburg, MD, United States, for the reference materials RM 8011–8013 [9], the Institute for Reference

Materials and Measurements, a Joint Research Centre of the European Commission, Geel, Belgium, for IRMM-304 [10] and the Microgenics Corporation (Thermo Scientific, formerly Duke Scientific), Fremont, CA, United States, for Duke 3050A, 3100A and 3200A [11].

Towards the end of 2008 each participant received an identical set of seven particle samples from METAS. In this way the comparison could proceed fully in parallel and no samples had to circulate. After initial sample preparation and evaluation tests, the participants were ready for comparison measurements at the beginning of 2010. The measurement period was initially planned to be 3 months and was finally extended to 4 months until the end of April 2010. INRIM joined the comparison in January 2011 when a draft report stating the measurement results was already available and therefore the INRIM results, while presented here, were not included for the reference value calculations.

3. Participants and methods

The participating NMIs applied seven different measurement setups each independently and directly traceable to the SI unit metre. The majority of the instruments are unique and partly built by the NMIs themselves. In the following, the instruments and the measurement procedures are presented.

3.1. PTB-SAXS

SAXS is an ensemble method like DLS. The nanoparticles in liquid suspension can directly be investigated without deposition onto a surface. Compared to DLS, the wavelength of the radiation is about four orders of magnitude shorter, thus perfectly suited for investigations on the nanoscale. For SAXS, intense monochromatic x-rays of low divergence are required, which are available at synchrotron radiation facilities. PTB operates a synchrotron radiation laboratory at the electron storage ring BESSY II in Berlin [12]. At the four-crystal monochromator beamline, any photon energy in the range from 1.75 to 10 keV, corresponding to wavelengths between 0.7 and 0.12 nm, can be selected by using either InSb (1 1 1) or Si (1 1 1) crystals in the monochromator. Different motor-controlled sets of slits in this 37 m long UHV beamline are used to produce a well-defined monochromatic photon beam with a diameter of approximately 0.5 mm and a spectral resolving power in the order of 10^4.

The undiluted suspensions were injected into glass capillaries with a diameter of 1 mm and a wall thickness of 10 μm. Up to 15 capillaries can be loaded via a load-lock into a UHV reflectometer, which allows for the rotation and the translation of the samples with all degrees of freedom. The last guard slit is already in the reflectometer, only a few centimetres in front of the sample. Directly behind the reflectometer, the SAXS setup of the Helmholtz-Zentrum Berlin (HZB) is installed. It mainly consists of a 3 m long, adjustable and tiltable support structure, and a CCD-based detector of 165 mm diameter with a nominal pixel size of 80 μm. Long edge-welded bellows with an inner diameter of 250 mm are used to vary the distance between the sample and the detector continuously without breaking the vacuum. The direct beam is blocked by a square beamstop with an area of 1 cm^2. The SAXS setup and the reflectometer are placed on motorized platforms for alignment with respect to the incoming beam. The entire beamline, including the monochromator, mirrors, slit systems, the reflectometer and the SAXS setup, is completely computer-controlled. The incident photon flux and the sample transmittance are measured by means of calibrated semiconductor photodiodes.

For the traceable size determination of nanoparticles, the position of the maxima and minima on the momentum transfer axis has to be known precisely, whilst a calibration of the scattered intensity is not required. For the momentum transfer, defined as $q = 4\pi/\lambda \cdot \sin\Theta$, the angle Θ (being half of the scattering angle) and the x-ray wavelength (λ) have to be traceable. For the wavelength, back-reflection of radiation from silicon crystals was used, relating the wavelength (or photon energy) scale of the monochromator to the precisely known lattice constant of silicon. The resulting relative uncertainty of the wavelength is about 10^{-4}. For the scattering angle, the distance between the detector and the sample as well as the pixel size of the detector has to be known. Both values can be determined by using features of the HZB SAXS setup. The pixel size is obtained by translations of the detector perpendicular to the beam direction. Pictures of the direct but strongly attenuated beam were taken at different displacements which can be measured precisely using a Heidenhain length encoder. A pixel size of 78.94 ± 0.04 μm was obtained, close to the manufacturer's specification. The distance cannot be measured directly, but strongly-structured scattering patterns can be recorded at different distances and the change of the distance can be measured with the built-in 3 m long Heidenhain encoder with an uncertainty of 20 μm. By triangulating to the source point, the sample–detector distance can be determined with an uncertainty of a few millimetres. The total relative uncertainty for the distance and the pixel size is about 0.5% [13, 14].

In a scattering pattern, concentric rings are observed as shown in figure 2. The square is the shadow of the beamstop placed in front of the detector to block the direct beam transmitted through the sample. From each picture, a dark image was first subtracted to remove the readout noise of the camera. To subtract a background image of a capillary filled with distilled water, the images were normalized to the measurement time, the incident beam intensity and the transmittance of the sample. The traces of cosmic rays were removed, the centre was determined and the flat image was projected to a spherical surface. Then the data were circularly integrated to obtain the scattered intensity as a function of the momentum transfer. The results are presented in figure 3 together with a fit using the software SASfit [15]. From this fit, the mean particle diameter and the distribution width were obtained. The assumption of a hard sphere model, which is well suited for all gold and the silica particles, turned out to be inapplicable for the large polymer particles. Very good fit results were instead obtained by using a core shell model, where the core diameter, its distribution width and the shell thickness were free parameters. As the physical meaning of the

Table 3. PTB-SAXS uncertainty contributions $u(x_i)$ with distribution (N = normal, R = rectangular) and contribution type (A or B) according to GUM [16], sensitivity coefficients c_i and estimated combined standard uncertainty $u_c(d)$ with its components $u_i(d)$ for the 100 nm polymer particles.

Input quantity x_i	Distrib./type	$u(x_i)$ unit	c_i	$u_i(d)$ (nm)
Photon energy	N/B	0.8 eV	0.0175 nm eV^{-1}	0.014
Pixel size	N/B	0.079 μm	1.65×10^{-3}	0.13
Sample detector distance	N/B	0.012 m	4.42×10^{-8}	0.53
Fit of diameter	N/A	1.9 nm	1	1.9
Shell thickness	N/A	1.4 nm	1	1.4
Combined standard uncertainty			$u_c(d) = 2.4$ nm	

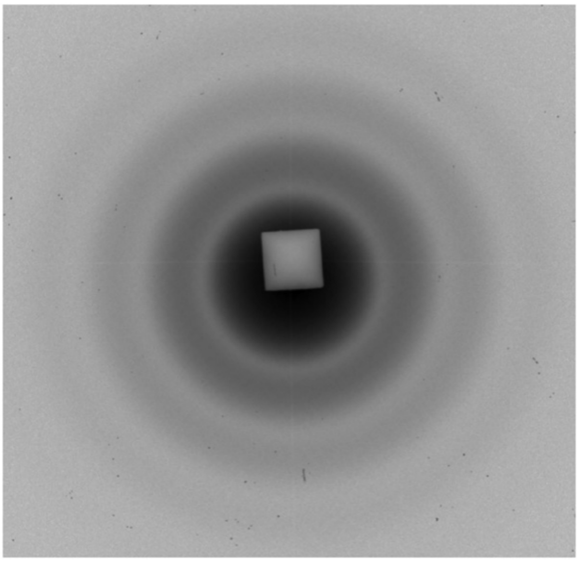

Figure 2. Scattering pattern obtained from nominally 60 nm gold particles in liquid suspension; photon energy: 8.0 keV, sample to detector distance: 3.0 m. The square is the shadow of the beamstop.

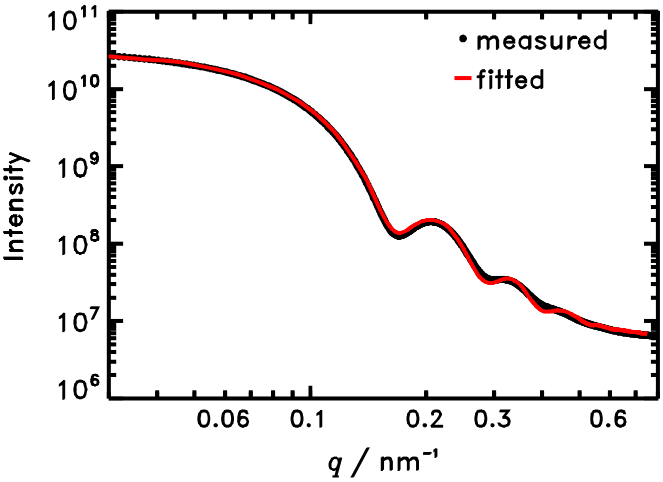

Figure 3. Scattered intensity obtained from figure 2 by circular integration together with the fitted curve, resulting in a number-weighted mean particle diameter of 52.8 ± 0.5 nm and a distribution width of 9 nm.

shell is not yet clear, the core diameter plus one shell thickness was used as the particle diameter, while one shell thickness was added to the uncertainty (table 3).

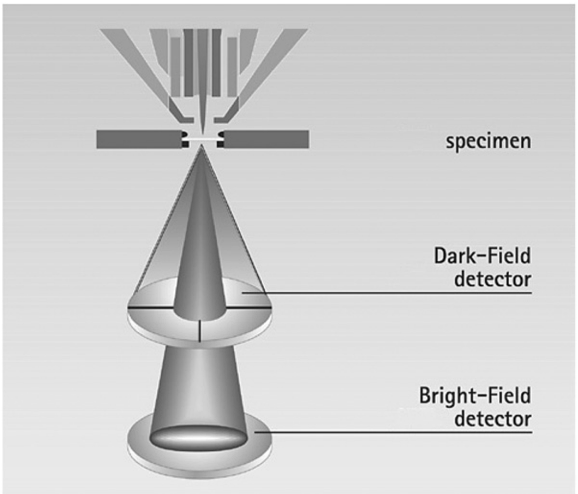

Figure 4. The transmission detector consists of five solid state detector segments, four of which are used for dark field imaging, by courtesy of Zeiss.

3.2. PTB-TSEM

Scanning electron microscopy in transmission mode (TSEM) combines the overall versatility of a SEM with (almost) TEM-like imaging and resolution. The basics of the technique are reviewed in [17]. Its use for highly accurate, traceable measurements of nanoparticle size is summarized below. A detailed description can be found in [18].

The experimental setup is presented in detail in [19]. It consists of a standard SEM (Zeiss Supra 35 VP) equipped with a commercially available transmission detector, see figure 4. Four solid state detector segments in the upper plane may be used for dark field imaging. Bright field imaging is enabled by a fifth detector segment which is placed underneath a small pinhole.

The instrument was calibrated using a two-dimensional grating of aluminium bumps on silicon. Its mean pitch of approximately 144 nm was traceably measured by deep UV laser diffraction [20]. The same SEM parameters are used during calibration and subsequent measurements.

Sample preparation took place in a cleanroom environment. One drop of undiluted nanoparticle suspension was given on TEM grids placed in the moulds of a Teflon plate. Subsequently the grids were stored for a period of time at 100% humidity before the liquid was removed gently by means of cleanroom tissue.

Table 4. PTB-TSEM uncertainty contributions $u(x_i)$ with distribution (N = normal, R = rectangular) and contribution type (A or B) according to GUM [16], sensitivity coefficients c_i and estimated combined standard uncertainty $u_c(d)$ with its components $u_i(d)$ for the 100 nm polymer particles.

Input quantity x_i	Distrib./type	$u(x_i)$ unit	c_i	$u_i(d)$ (nm)
Pixel pitch in the x-direction	N/B	0.006 nm	11	0.07
Pixel pitch in the y-direction	N/B	0.011 nm	11	0.12
Threshold level simulation	R/B	0.018	42 nm	0.75
Signal level at particle centre	N/B	500 grey levels	0.0002 nm	0.08
Background signal level	N/B	500 grey levels	0.001 nm	0.48
Pixel noise	N/B	8 pixel	0.004 nm	0.03
Image analysis parameters	N/B	1.5 nm	1	1.50
Digitization	N/B	0.9 nm	1	0.90
Statistics	N/A	5.2 nm	0.027	0.14
Combined standard uncertainty			$u_c(d) = 2.0$ nm	

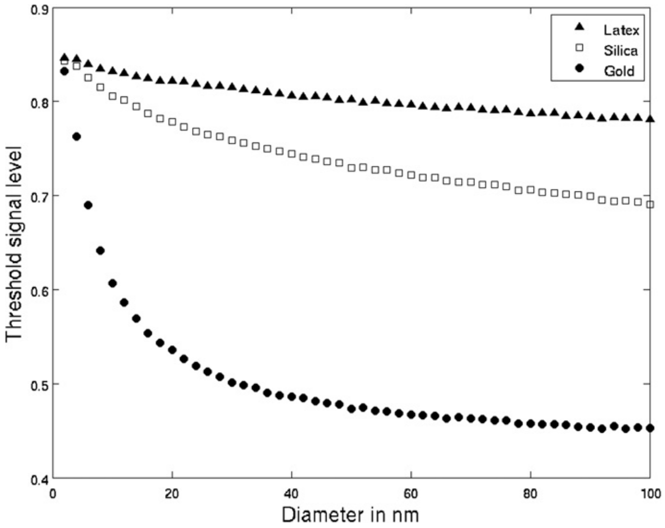

Figure 5. The threshold signal level at the particle boundary depends on both material and size of the particle.

An automated image acquisition routine has been developed which processes an externally generated list of measurement positions. Thanks to the resulting speedup at least 200 bright field images from at least two TEM grids could be taken for each particle sample.

Highly accurate size measurements of nanoparticles rely on a precise determination of the particle boundary in the TSEM image. If simple thresholding approaches are used to separate the particles from the background the size distribution changes depending on the chosen algorithm [21]. Meaningful threshold signal levels at the particle boundary can be determined using Monte Carlo simulations of the physical effects involved in TSEM image formation [22]. As a result the threshold level at the particle boundary depends on both material and size of the particle as can be seen in figure 5. Taking this into account, an automated image analysis has been developed which determines the particle size iteratively. Based on a first guess of the size the threshold level is determined which leads to an improved estimation of the size and so on.

Due to the need to separate particles from artefacts such as dirt, image analysis is the biggest contributor to the overall uncertainty (table 4). Other large contributions arise from digitalization and from the determination of the threshold signal levels at the particle boundary because the parameters of the simulation are only known within certain limits. Further contributions do play minor roles. These are effects of statistics, grey scale values, calibration and pixel noise. While great care has been taken to prepare representative subsamples, the effect of sample preparation cannot be currently verified and these effects are therefore not included in the stated uncertainty values.

3.3. INM-SEM

The SEM technique was applied using a Quanta Inspect F Electron Microscope, manufactured by FEI, fitted with a field emission electron source and an Everhart–Thornley detector for secondary electrons and a detector for backscattered electrons. The maximum electron energy is 30 keV and the achievable resolution is specified to be 1.4 nm. Equipment maintenance and adjustments was undertaken by the manufacturer based on their working instructions and the relevant international procedures [23]. Magnification reference standards certified by Geller Microanalytical Laboratory, traceable to NPL, were used for calibrating the SEM magnification of the x- and y-scales. The same SEM parameters were used during calibration and the subsequent measurements.

Undiluted samples were used and ultra-sonication was only used for the gold sample of 10 nm. The conductive specimens, that are the gold samples, were loaded onto a copper grid covered with lacy carbon film and imaged using backscattered electrons. The non-conductive specimens, that is the colloidal silica and the polymer samples, were loaded onto an aluminium disc and analysed by secondary electron imaging. The samples were gently dried in air for about 20–30 min on the carbon grid or on the aluminium disc, using the weak temperature rise obtainable under an optical microscope due to its illumination. The SEM parameters were optimized and images captured for the subsequent particle size measurement and size distribution analysis.

About 10 μL of the sample solution was used for all SEM investigations. The gold nanoparticle samples were used just after opening the original ampoules, while the colloidal silica sample and the polymer samples were opened 6 months before the SEM investigations. To ensure that the specimen under

Table 5. INM-SEM uncertainty contributions $u(x_i)$ with distribution (N = normal, R = rectangular) and contribution type (A or B) according to GUM [16], sensitivity coefficients c_i and estimated combined standard uncertainty $u_c(d)$ with its components $u_i(d)$ for the 100 nm polymer particles.

Input quantity x_i	Distrib./type	$u(x_i)$ unit	c_i	$u_i(d)$ (nm)
Repeatability of mean diameter d	N/A	0.0056	D	0.56
Image evaluation	R/B	2.31 nm	1	2.31
SEM calibration	R/B	0.0058	d	0.58
Measurement conditions	R/B	0.0058	d	0.58
Combined standard uncertainty			$u_c(d) = 2.51$ nm	

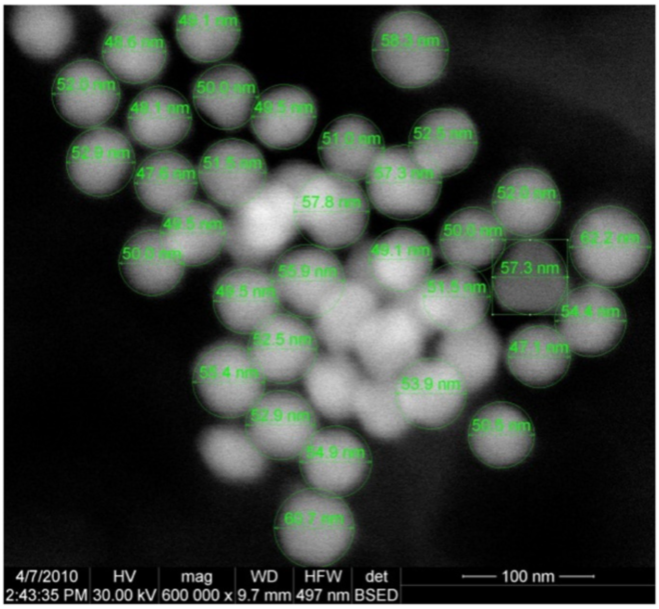

Figure 6. SEM image of gold spheres (NIST RM 8013) having a nominal diameter of 60 nm.

investigation is representative and that the statistical errors due to inadequate representation are controlled, the samples were well dispersed on the copper grid or aluminium disc and a sufficient number of particles was counted (at least 100 particles were observed).

SEM image evaluation was performed by determining the particle size as the diameter of a sphere that has the same projected area. About 100 particles were measured so the mean value was estimated from several images of each sample. The measurement uncertainties reported here were estimated considering all known variation sources (table 5). The overall repeatability, especially due to the detection of the particle edges in the images, was the main source of uncertainty. Other components were the variations associated with the equipment (i.e. 5% from the measured value, as specified by manufacturer), the laboratory environmental conditions (i.e. temperature, humidity) and the nature of the specimens under investigation. An image of gold spheres having a nominal diameter of 60 nm is shown in figure 6.

3.4. METAS-AFM

The measurements were made using a modified ‘Dimension 3500’ metrology AFM from Digital Instruments. The AFM head has parallelogram flexures and uses capacitive sensors for the tip displacement measurement. The sensors are traceable to the definition of the metre through an interferometric calibration in the z-direction and laterally by using reference gratings calibrated by laser diffraction at METAS [24]. In order to confirm the results for the 200 nm polymer spheres, additional measurements were made using a new, just recently built, 3D-AFM having three differential interferometers.

All particles were deposited on freshly cleaved, atomically flat mica surfaces. The mica surfaces were pretreated with poly-L-lysine except for the two larger polymer particle samples which formed hexagonal ordered particle layers. All samples, except the gold colloids, were diluted using ultrapure water. AFM images with various ranges were made in order to check that no height information was lost by the image resolution of usually 512 × 512 pixels. Also scan speed and other parameters were tested for their respective influence. Several images were acquired for each particle type to ensure that finally several hundred particles contribute to a mean diameter value.

On all samples the particle heights were measured with respect to the atomically flat mica reference surface. For two samples, the 100 and 200 nm polymer spheres, lateral measurements on hexagonal ordered particle layer were also made. These lateral results were not included in the comparison and they were only used to confirm the height values reported here. All measurements were carried out in a temperature controlled laboratory in the basement of METAS. The applied AFM particle size measurement method is well established at METAS [25, 26]. All data evaluations were made using Scanning Probe Image Processor SPIP [27] and were partly verified by self-made AFM image evaluation software.

The uncertainty estimation considered nine contributions. The largest ones were the tip–sample interaction (tapping setpoint) and the estimated background flatness (scanner and mica). Other minor contributions were the AFM z-calibration, the capacitive sensor nonlinearity, evaluation parameters, sample homogeneity, noise and repeatability (table 6).

The 100 and 200 nm polymer particles formed a hexagonal ordered particle layer. Locations with narrow stripe-like depositions were preferred for the measurements (figure 7). Using images from such locations both lateral distances and particle height values could be evaluated using exactly the same particles. Due to the size variation of the particles the hexagonal ordered particle layer cannot be closely packed and lateral gaps can be observed [28]. The lateral measurements were corrected using a particle packing model proposed earlier by METAS. A simple numerical simulation revealed that

Table 6. METAS-AFM uncertainty contributions $u(x_i)$ with distribution (N = normal, R = rectangular) and contribution type (A or B) according to GUM [16], sensitivity coefficients c_i and estimated combined standard uncertainty $u_c(d)$ with its components $u_i(d)$ for the 100 nm polymer particles.

Input quantity x_i	Distrib./type	$u(x_i)$ unit	c_i	$u_i(d)$ (nm)
Mean particle height	N/A	0.16 nm	1	0.16
Probe interaction (tapping SP)	R/B	0.58 nm	1	0.58
Evaluation settings and filters	R/B	0.20 nm	1	0.20
z-calibration linear	R/B	0.0006	d	0.06
z-calibration nonlinear	R/B	0.0043	d	0.43
Sample preparation	R/B	0.12 nm	1	0.12
Substrate flatness	R/B	1.73 nm	1	1.73
Scanner hysteresis	R/B	0.002	d	0.20
Noise and vibration	R/B	0.12 nm	1	0.12
Combined standard uncertainty			$u_c(d) = 1.91$ nm	

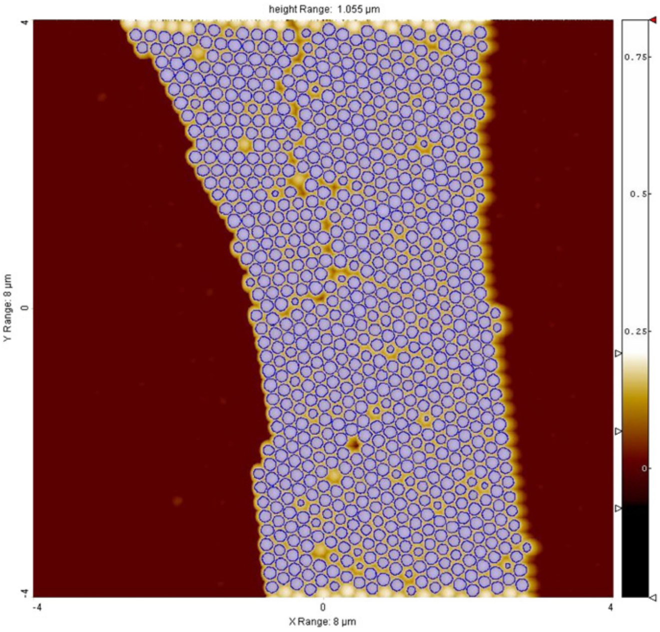

Figure 7. AFM measurement of 200 nm polymer particles (Duke 3200A) which formed a hexagonal ordered particle layer. Image size: 8 μm × 8 μm, 1024 × 1024 pixels. Height evaluation using SPIP [27].

the average particle distances are about 1/3 of the particle standard deviation too big. The standard deviation of the height distribution was therefore used to correct the lateral spacing. The lateral spacing of the Duke 3200A sample was 196.1 nm before and 194.0 nm after packing correction, very close to the measured height value of 194.4 nm.

3.5. MIKES-AFM

At MIKES the measurements were carried out using a Park XE-100 AFM. The instrument has been carefully characterized [29]. Before and after the measurements the x- and y-scales of the AFM were calibrated with a 1D grating which in turn was calibrated by means of a laser diffractometer at MIKES [30]. The z-scale was calibrated using step height standards which were calibrated with the MIKES interferometrically traceable metrological AFM (IT-MAFM) [31]. The measurements were carried out in a temperature controlled laboratory on a table with active vibration isolation [32]. Non-contact mode was used for all measurements.

The sample preparation methods were similar to those described for METAS. The smallest polymer particles (Duke 3050A) were not measured because of problems in sample preparation.

Measurement ranges were adjusted to fit the size of the particles from 1 μm × 1 μm for the smallest gold particles to 10 μm × 10 μm for the largest polymer particles. Pixel amounts in the measurements were 1024 × 1024 or 512 × 512. Two images were analysed for each of the gold and silica samples. One image was selected for analysis of each of the polymer particle samples. The data analysis was made using SPIP software [27].

The diameters of the silica and gold particles were determined from the height of single particles. Several heights were measured to determine the average diameter and the size distribution. Numbers of measured particles range from 19 to 160.

The diameters of the polymer particles were determined from the lateral spacing. Using AFM images of areas where particles formed a hexagonal ordered particle layer, lines with particles in good order were selected. The length of a particle row was determined and divided by the particle number to obtain the mean diameter. The size distribution was calculated from the height variation of the particles.

The main uncertainty component in measurements of gold and silica particles came from the particle height measurement including the detection of the highest point on the particles, flatness error of the mica surface and the uncorrected nonlinearity of the movement in the z-direction. Another large uncertainty component was the repeatability of the measurement. The repeatability component included errors caused by particle size distribution, sampling and particle shape. The other error components were tip–sample interaction, sample preparation and calibration of the z-scale.

The main uncertainty component in measurements of polymer particles is the correction of the lattice spacing due to the size variation of the particles (table 7). The correction was estimated from the size distribution by comparing the mean values calculated from all data (d_{all}) and cutting the smallest and largest particles (d_{cut}). This is done because the smallest or largest particles are not seen in the mean values measured

Table 7. MIKES-AFM uncertainty contributions $u(x_i)$ with distribution (N = normal, R = rectangular) and contribution type (A or B) according to GUM [16], sensitivity coefficients c_i and estimated combined standard uncertainty $u_c(d)$ with its components $u_i(d)$ for the 100 nm polymer particles.

Input quantity x_i	Distrib./type	$u(x_i)$ unit	c_i	$u_i(d)$ (nm)
Calibration of the standard	N/B	0.000 05	d	0.01
Calibration of the AFM	N/B	0.001	d	0.1
Detection of particles	N/B	0.5 nm	1	0.5
Sample preparation	N/B	0.3 nm	1	0.3
Spacing correction	N/B	0.6 nm	1	0.6
Repeatability	N/A	0.7 nm	1	0.7
Combined standard uncertainty			$u_c(d) = 1.1$ nm	

Table 8. INRIM-AFM uncertainty contributions $u(x_i)$ with distribution (N = normal, R = rectangular) and contribution type (A or B) according to GUM [16], sensitivity coefficients c_i and estimated combined standard uncertainty $u_c(d)$ with its components $u_i(d)$ for the 100 nm polymer particles.

Input quantity x_i	Distrib./type	$u(x_i)$ unit	c_i	$u_i(d)$ (nm)
Repeated observations $u(d)$	N/A	1.2 nm	1	1.2
Z interferometric calibration	N/A	0.03	d	3
Pixel resolution	R/B	0.5 nm	1	0.5
Z-resolution 16 bit ADC	R/B	0.1 nm	1	0.1
Noise	N/A	0.5 nm	1	0.5
Reference plane	R/B	0.6 nm	1	0.6
Tip geometry	R/B	0.2 nm	1	0.2
Particles size distr. and shape	R/B	1.2 nm	1	1.2
Combined standard uncertainty			$u_c(d) = 3.6$ nm	

from the lattice structure. There is empty space around the smallest particles and the largest particles cause dislocations in the lattice. The correction $d_{\text{all}} - d_{\text{cut}}$ was –1.75 nm (u_c = 0.9 nm) for the 200 nm polymer particles. For the 100 nm polymer particles the error was not corrected but it was taken as an uncertainty component (u_c = 0.6 nm). Also in this measurement, repeatability was the most important uncertainty component. Other smaller uncertainty components came from calibration of the AFM, detection of the position of the particles and sample preparation.

3.6. INRIM-AFM

Measurement runs were carried out using an AFM based on a sample-moving scanning system with interferometric closed-loop control of *xy*-displacements and an open-loop *z*-stage. The *z* scanning system was calibrated off-line using an interferometric setup. The microscope makes use of an AFM head operating in intermittent mode. Commercially available non-contact AFM tips were used. The microscope is located in a temperature controlled laboratory in the basement of INRIM.

The sample preparation methods were similar to those described for METAS. Several AFM images, mainly with 1024 × 1024 pixel resolution, were taken from different areas on each sample.

Using the 200 nm polymer spheres, several AFM images of hexagonal ordered particle layers were taken (figure 8). The mean diameter of these particles was determined by lateral measurements using two different methods. The first was based on autocorrelation and unit cell detection in the image, whereas the second was based on distance measurements along lines of packed particles.

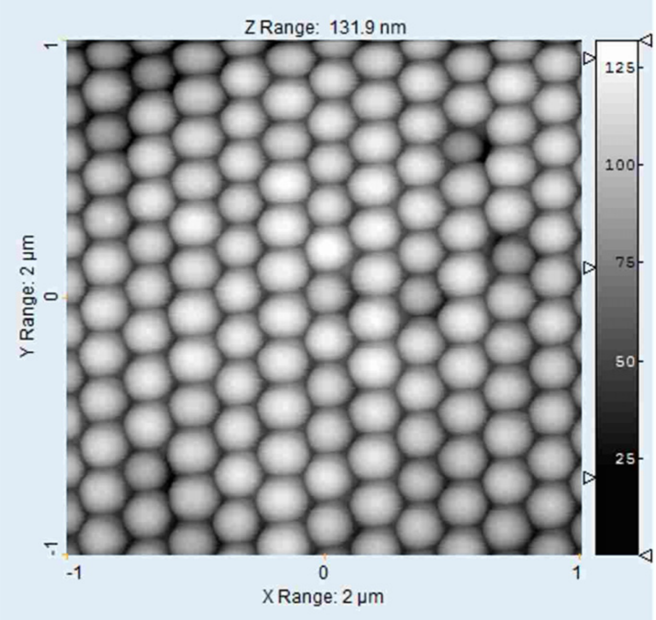

Figure 8. AFM image of polymer spheres having a nominal diameter of 200 nm.

For all other samples the mean diameter of particles has been determined from height profiles across isolated particles with respect to the substrate. Data evaluation was performed using the SPIP software tool [27]. The overall repeatability including the size distribution obtained from several images of each sample resulted as a main component of the estimated uncertainty (table 8). Other components are from the instrument calibration (lateral or vertical sizes depending on the measurement method), reference plane, noise and other minor terms.

3.7. NPL-DLS

When coherent light is scattered by a suspension of nanoparticles in a liquid, variations or 'speckles' in the intensity of the scattered light are seen. These are caused by differences in the phases of the waves scattered by different particles. By monitoring these speckles in the light passing through a small pinhole (smaller than the size of the speckle) it is possible to tell how fast the scattering particles are diffusing over a distance equal to the wavelength of scattered light. The raw data from the DLS experiment is in the form of time-averaged autocorrelation data, which contain information on all the diffusional timescales present in the system [33]. For mono dispersed particles in suspension then the correlation is dominated by an exponential decay with rate (Γ) given by

$$\Gamma = Dq^2, \tag{1}$$

with D being the diffusion coefficient of the nanoparticles and q the scattering vector given by

$$q = \frac{4\pi n}{\lambda} \sin\left(\frac{\theta}{2}\right), \tag{2}$$

where n is the refractive index of the suspension medium, λ the wavelength of the incident light and θ is the scattering angle. Hence, from the correlation curve the diffusion coefficient can be determined. The hydrodynamic diameter d of the particles can then be simply determined from the diffusion coefficient D using the 'Stokes–Einstein' relationship.

$$d = \frac{kT}{3\pi\eta D}, \tag{3}$$

where k is the Boltzmann constant, η is the solvent viscosity and T is the absolute temperature. This technique is extremely precise when there is a simple distribution of decay times, e.g. for scattering from spherical nanoparticles with a narrow distribution of sizes about a single mean.

For polydisperse samples this simple approach has to be modified. The method of cumulants [34] is now commonly used, where the natural log of the autocorrelation function is expanded into a power series. Due to the limitations of the DLS technique this is normally truncated for powers greater than 2, leading to a quadratic cumulant expression. From this the mean decay rate (and particle size) and the polydispersity index, which gives an indication of the polydispersity present in the sample, can be obtained. It is usually a good assumption to assume that nanoparticle samples follow a log-normal distribution [35] and the first two moments of the autocorrelation function are enough to compute the moments of the particle log-normal size distribution [36].

All DLS measurements were taken using a commercial instrument (Nanosizer, Malvern, UK) following the relevant international standard [37]. This instrument is fitted with a He–Ne laser, uses a scattering angle of 173° and is fitted with non-invasive backscatter detection technology to ensure that particle concentration does not affect the measurement. All measurements were taken at 20 ± 0.1 °C. The samples were supplied already dispersed in an aqueous suspension. Therefore sample preparation was minimal. The only requirement is dilution to the correct concentration. For the gold colloids this was done with 10 mmol NaCl solution in the ratio of 1:300 for RM 8011 and 1:400 for RM 8012 and RM 8013; the IRMM-304 sample was used undiluted. The latex spheres were diluted in ultrapure water in the ratios 1:5000, 1:4000 and 1:2000 for 3050A, 3100A and 3200A, respectively. 500 μL of each sample was measured in a single-use polystyrene half-micro curette with a path length of 10 mm. All measurements were made at a position of 4.65 mm from the curette wall with an automatic attenuator. For each sample 15 runs of 20 s were performed, with each run being repeated ten times. The software to collect and analyse the data was the Dispersion Technology Software (v6.01) (Malvern, UK).

Determining the uncertainty in DLS measurements is hampered by the lack of any direct transfer standards. An alternative approach, as developed by Takahashi *et al* [38], is to develop a model approach in accordance with the international document 'Guide to the expression of uncertainty in measurement' (GUM) [16]. From equations (1)–(3) it can be seen that there are many contributions to the measurement uncertainty, including those associated with the Boltzmann constant (k), temperature (T), viscosity (η) and refractive index of the suspension medium (n), wavelength of the laser (λ), setting of the scattering angle (θ), the decay rate (Γ) and the measurement repeatability. Combining these gives the expression of the uncertainty to be

$$u^2(d) = f^2\left[\frac{u^2(k)}{k^2} + \frac{u^2(T)}{T^2} + \frac{u^2(\eta)}{\eta^2} + \frac{u^2(\Gamma)}{\Gamma^2} + 4\left\{\frac{u^2(n)}{n^2} + \frac{u^2(\lambda)}{\lambda^2} + \frac{u^2(\theta)}{4\tan^2(\theta/2)}\right\}\right], \tag{4}$$

with

$$f = \frac{kT}{6\pi\eta(\Gamma/q^2)}. \tag{5}$$

The specific contributions to the uncertainty were determined as follows. The Boltzmann constant, k, and its related uncertainty were estimated according to the committee on Data for Science and Technology (CODATA, 2010). The temperature was measured directly using a calibrated thermocouple. The uncertainty related to the viscosity of the solvent has two contributions. The first contribution arises from the uncertainty of the viscosity of pure water at 20.0 °C, reported in ISO 3666 to be 0.000 85 mPa s, and the second from the variation in temperature determined according to equation (6):

$$\eta = A\exp\left[\frac{1 + BT}{CT + DT^2}\right], \tag{6}$$

where $A = 0.012\,571\,87$ mPa s, $B = -5.806\,436 \times 10^{-3}$ K^{-1}, $C = 1.130\,911 \times 10^{-3}$ K^{-1}, $D = -5.723\,952 \times 10^{-6}$ K^{-2}, and T = temperature in kelvin. The combined uncertainty of viscosity is the combination of the two contributions.

The uncertainty in the scattering angle was determined from the geometry of the system. The instrument uses the popular helium neon laser which has a wavelength of $\lambda_{\text{HeNe}} = 632.816$ nm in air. The actual wavelength lies within

Table 9. NPL-DLS uncertainty contributions $u(x_i)$ with distribution (N = normal, R = rectangular) and contribution type (A or B) according to GUM [16], sensitivity coefficients c_i and estimated combined standard uncertainty $u_c(d)$ with its components $u_i(d)$ for the 100 nm polymer particles.

Input quantity x_i	Distrib./type	$u(x_i)$ unit	c_i	$u_i(d)$ (nm)
Boltzmann constant	N/B	$2.3 \cdot 10^{-29}$ J K^{-1}	$7.7 \cdot 10^{24}$ nm K J^{-1}	$1.77 \cdot 10^{-4}$
Temperature	R/B	0.0577 K	0.36 nm K^{-1}	0.021
Viscosity	$^{\mathrm{N}}/_{\mathrm{R}}$/B	0.0014 mPa s	−125 nm mPa^{-1} s^{-1}	0.175
Wavelength of laser	N/B	$2.5 \cdot 10^{-11}$ m	−0.34	0.008
Refractive index	R/B	$6.35 \cdot 10^{-4}$	160.5 nm	0.101
Scattering angle	R/B	$2.52 \cdot 10^{-4}$ rad	35.4 nm rad^{-1}	0.009
Decay rate	N/B	3.27 10^{-7} s^{-1}	−1.06 10^{7} nm s	0.347
Repeatability	N/A	0.288 nm	1	0.288
Combined standard uncertainty			$u_c(d) = 0.494$ nm	

±0.001 nm of this value due to thermal expansion and contraction of the cavity. The refractive index of the liquid medium depends on the temperature, wavelength of the laser and its composition. For temperatures between 20 and 30 °C and with a laser wavelength of 633 nm, the refractive index of water can vary between 1.3324 and 1.3346 with an assumed rectangular distribution.

The uncertainty in the decay rate is a function of the square root of the ratio between the decay rate and sampling time [34]. Larger, slower moving particles will have a longer decay time, leading to increased uncertainty, compared to smaller particles for the same sampling time. The repeatability of the measurement (u_r) is the final contribution to the uncertainty that needs to be considered. This is determined by the standard deviation of the mean. Factors affecting the repeatability include particle–particle interactions and multiple scatterings of the same photon by different particles. For these latter reasons a lower concentration of particles is preferred. However reducing the concentration too much lowers the scattering intensity and the signal to noise ratio.

The calculation of the standard uncertainty for the sample of 100 nm latex particles is given in table 9. The major components are those associated with the determination of the decay rate and repeatability.

4. Calculation of comparison reference value and consistency check

4.1. Measurand

The measurand in this comparison was defined to be the mean diameter of the particles contained in each sample sent to the participants. A single particle diameter was defined as the diameter of a single sphere having the same volume as the particle. The mean diameter reported by the participants was defined to be the linear average of the individual particle diameters of all particles analysed (number-weighted average diameter).

The results should be given for the standard conditions, $T = 20$ °C, $H_{\mathrm{rel}} = 50\%$ and $p = 1013.25$ mbar. However, for the methods working in vacuum or in liquid no corresponding corrections were applied. It was required that the measurement uncertainty is calculated using all known influences such as contributions from particle shape, particle size distribution, sampling of the material, sample preparation and all contributions specific for the measurement method as well as deviations from the measurand definition.

If possible, the participants provided additional particle information such as the number of particles analysed, the standard deviation of the particle diameter distribution, the median value of the diameter distribution (middle value), the mode value of the diameter distribution (highest probability value) and the histogram of the size distribution.

4.2. Determination of intercomparison reference value

From the mean diameters d_i reported by the participants the reference values d_{ref} were calculated as the weighted mean with the weights based on the corresponding estimated uncertainties $u(d_i)$. The weights used are $u^{-2}(d_i)$ (equation (7)). The uncertainty of the reference value $u_c(d_{\mathrm{ref}})$ is calculated using equation (8).

$$d_{\mathrm{ref}} = \frac{\sum_{i=1}^{n} u^{-2}(d_i) \cdot d_i}{\sum_{i=1}^{n} u^{-2}(d_i)}, \tag{7}$$

$$u_c(d_{\mathrm{ref}}) = \left(\sum_{i=1}^{n} u^{-2}(d_i) \right)^{-1/2}, \tag{8}$$

$$U_{95}(d_{\mathrm{ref}}) = u_c(d_{\mathrm{ref}}) \cdot k_{95} \quad \text{with} \quad k_{95} = 2. \tag{9}$$

The expanded uncertainty U_{95} (equation (9)) has also been calculated, taking into account the actual degrees of freedom provided by the participants. Since the differences are negligible, $k_{95} = 2$ is used here for simplicity.

The Birge ratio [39] was used to test the results for statistical consistency. The Birge ratio compares the observed spread of results with the spread of the estimated uncertainty (equations (10)–(12)). $R_B > 1$ indicates an underestimation of measurement uncertainty, while $R_B < 1$ indicates an overestimation of measurement uncertainty.

$$R_B = \frac{u_{\mathrm{ext}}}{u_{\mathrm{in}}} \tag{10}$$

with

$$u_{\mathrm{ext}} = \sqrt{\frac{\sum_i ((d_i - d_{\mathrm{ref}})/u(d_i))^2}{(n-1) \cdot \sum_i u(d_i)^{-2}}} \tag{11}$$

Table 10. Mean diameter d_{mean} and combined standard uncertainty u_c for the seven nanoparticle samples as reported by the participants.

Participant	NIST RM 8011 $d_{\mathrm{mean}} \pm u_c$ (nm)	NIST RM 8012 $d_{\mathrm{mean}} \pm u_c$ (nm)	NIST RM 8013 $d_{\mathrm{mean}} \pm u_c$ (nm)	IRMM-304 $d_{\mathrm{mean}} \pm u_c$ (nm)
PTB-SAXS	8.84 ± 0.25	25.3 ± 0.5	52.8 ± 0.5	25.7 ± 0.3
PTB-TSEM	9.1 ± 0.6	27.9 ± 0.6	57.1 ± 1.2	27.5 ± 0.9
INM-SEM	6.70 ± 2.31	26.10 ± 2.89	54.30 ± 2.37	35.3 ± 2.42
METAS-AFM	7.25 ± 0.84	24.24 ± 0.87	53.06 ± 0.94	24.04 ± 0.88
MIKES-AFM	8.56 ± 1.90	22.96 ± 1.3	57.45 ± 2.20	25.96 ± 1.30
INRIM-AFM	7.8 ± 1.2	24.6 ± 1.8	49.4 ± 3	27.5 ± 4
NPL-DLS	11.65 ± 0.18	37.70 ± 0.68	65.67 ± 0.31	40.83 ± 0.15
Participant	Duke 3050A $d_{\mathrm{mean}} \pm u_c$ (nm)	Duke 3100A $d_{\mathrm{mean}} \pm u_c$ (nm)	Duke 3200A $d_{\mathrm{mean}} \pm u_c$ (nm)	
PTB-SAXS	47.2 ± 1.1	96.0 ± 2.4	200.5 ± 3.5	
PTB-TSEM	44.5 ± 1.3	98.9 ± 2.0	201 ± 2.3	
INM-SEM	44.70 ± 2.38	98.10 ± 2.51	190.00 ± 2.86	
METAS-AFM	44.98 ± 0.90	91.92 ± 1.91	194.40 ± 2.11	
MIKES-AFM	–	99.52 ± 1.10	201.76 ± 1.30	
INRIM-AFM	38.7 ± 2.5	87.4 ± 3.6	186.3 ± 4.1	
NPL-DLS	56.13 ± 0.32	106.09 ± 0.49	200.46 ± 1.21	

and

$$u_{\mathrm{in}} = \left(\sum_{i=1}^{n} u^{-2}(d_i)\right)^{-1/2} = u_c(d_{\mathrm{ref}}), \tag{12}$$

where u_{ext} expresses a weighted standard deviation of the results d_i.

Assuming that the measurement results are normally distributed, the quantity $(n-1)R_B^2$ has a chi-square distribution (χ^2) with $(n-1)$ degrees of freedom, see e.g. [40]. Hence, the 95% one-sided confidence interval for R_B is given by

$$R_B < \sqrt{\frac{\chi^2_{0.05,\nu}}{\nu}}; \tag{13}$$

$\nu = n - 1$, and $n =$ number of participants.

Thus, the Birge ratio R_B has to meet the criterion (13) to fulfil the statistical consistency test. Here, the one-sided test was used because we are interested in noticing significant underestimations of uncertainty. The consistency of an individual measurement result with the corresponding reference value was verified using the En_{95} value. The En_{95} value is the ratio between the deviation to the reference value and the uncertainty of this difference (equation (14)) at a confidence level of 95% ($k = 2$). The minus sign ($-$) is used in the denominator for values contributing to the reference value and a plus sign ($+$) for values not contributing to the reference value (correlation). $|\mathrm{En}_{95}| > 1$ indicates possible inconsistencies.

$$\mathrm{En}_{95}(d_i) = \frac{d_i - d_{\mathrm{ref}}}{2 \cdot \sqrt{u_c^2(d_i) \mp u_c^2(d_{\mathrm{ref}})}}. \tag{14}$$

5. Results

5.1. Size measurements from different institutes

The seven participating laboratories from six NMIs delivered results for the mean particle diameter of seven samples giving a total of 48 results. The mean diameter and the combined standard uncertainty for the seven particle samples are listed in table 10. The results were obtained from seven different instruments. PTB supplied two measurement results for the two independent measuring techniques SAXS and TSEM. The other methods used were AFM, DLS and SEM giving a total of five different methods. MIKES reported problems with the preparation of the Duke 3050A sample and therefore delivered only six results.

5.2. Determination of reference value using the Birge criterion

For the calculation of the reference values all available results were used, except those from the DLS method, which represent hydrodynamic diameters as discussed below, the post-deadline results of INRIM, which were received 1 year after the other results, and the single result from INM-SEM for IRMM-304, which was identified to be a clear outlier. In total 33 results were accepted to contribute to the reference values.

For four out of the seven samples the Birge ratio did not meet condition (13) which indicates that some of the uncertainties have been underestimated or that some of the data contain systematic errors. Applying the rule of eliminating results until the Birge criterion [39] is fulfilled would have excluded 7 of the 33 values. Valuable measurements, with slightly too small uncertainties, would have been lost for these four reference value calculations. The main goal of this comparison was rather to deliver a set of particles with reliable reference values of small uncertainties than to validate the estimated individual uncertainties of the participants. To achieve this goal an additional uncertainty contribution due to unknown effects was included for each of the measurement results of these four samples before the reference values were calculated. This approach means that in these cases d_{ref} in equation (7), $u_c(d_{\mathrm{ref}})$ in (8) and EN_{95} in (14) were calculated using $u_c(d_i)$ values which include an unknown contribution u_{unknown}. This contribution varied from 0 to 4.46 nm depending on the sample and was set iteratively to fulfil the Birge criterion with $R_B = 1$, i.e. we determined the value of an unknown uncertainty to achieve consistency. By this measure no further exclusions were necessary and

Table 11. Comparison reference values for the particle diameter, uncertainty, expanded uncertainty and minimum unknown uncertainty contribution to achieve consistency.

	NIST RM 8011	NIST RM 8012	NIST RM 8013	IRMM-304	Duke 3050A	Duke 3100A	Duke 3200A
d_{ref} (nm)	8.74	25.37	54.55	25.72	45.51	97.03	197.68
$u_c(d_{\mathrm{ref}})$ (nm)	0.22	0.87	0.99	0.27	0.59	1.42	2.27
U_{95} (nm)	0.44	1.74	1.99	0.53	1.19	2.84	4.54
u_{unknown} (nm)	0	1.60	1.76	0	0	2.50	4.46

Table 12. Consistency of the results expressed as $|\mathrm{En}_{95}|$ values. The values which were not used for the reference value calculation are marked with an asterisk. $|\mathrm{En}_{95}| > 1$ are bold.

Participant	NIST RM 8011	NIST RM 8012	NIST RM 8013	IRMM-304	Duke 3050A	Duke 3100A	Duke 3200A
PTB-SAXS	0.41	0.02	0.57	0.06	0.91	0.16	0.27
PTB-TSEM	0.32	0.86	0.68	**1.04**	0.44	0.33	0.37
INM-SEM	0.44	0.11	0.05	**1.97***	0.18	0.17	0.80
METAS-AFM	0.92	0.35	0.43	1.00	0.39	0.91	0.37
MIKES-AFM	0.05	0.64	0.55	0.10	–	0.53	0.50
INRIM-AFM	0.39*	0.19*	0.81*	0.22*	**1.33***	**1.24***	**1.21***
NPL-DLS	**5.11***	**5.59***	**5.34***	**24.81***	**7.86***	**3.02***	0.54*

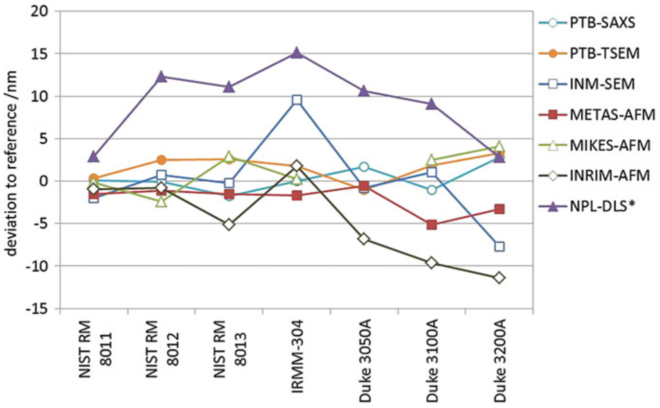

Figure 9. Deviations of individual particle diameter measurements from the corresponding comparison reference values.

the comparison reference values gained in stability and consistency. The comparison references values are displayed in table 11 where the calculations for four samples include unknown contributions. The deviations of all individual results from the determined comparison reference values are shown in figure 9.

Sources for the unknown uncertainty contribution could arise from effects which are difficult to access and which, therefore, were not included in the individual uncertainty budgets. Examples of such uncertainty contributions include sample preparation, influence of the surrounding media, air pressure, humidity, clustering and unexpected particle size distributions. The advantage of using an unknown uncertainty contribution is that all reference values with their uncertainties are valid and rely on the broadest base of measurements.

Although the Birge criterion is fulfilled for all samples, some $|\mathrm{En}_{95}|$ values can still be slightly greater than 1. This is the case for one of the 33 consistent values used for reference value calculation and for nine values which did not contribute to the reference values, see table 12.

6. Discussion

Figure 10 visualizes the measurement values (table 10) as well as the reference values (table 11) together with the particle diameters as stated by the manufacturers. DLS always measured mean diameter values significantly higher than the other methods, but the values provided by NPL are consistent with DLS measurements of the suppliers in the case of silica and the largest latex particles. Whilst this phenomenon needs to be investigated further, there are several factors that can cause this. DLS determines the equivalent translatory diffusion hydrodynamic radius while SEM, TSEM and AFM determine geometrical diameters. The hydrodynamic diffusion diameter is very sensitive to the presence of double layers. Additionally, the size measured is intensity weighted rather than number weighted as for other techniques [37]. This makes it extremely sensitive to even a small number of agglomerates. It can be shown that the presence of only 1% of the particles being present in the form of agglomerates is enough to explain the discrepancies between DLS and the other techniques [41].

For the gold particles, NIST states method-dependent particle sizes accompanied with measurement uncertainties. The uncertainties are based solely on statistics for SEM, TEM and DLS [9] and on ‘within-method-uncertainty’ [42] for AFM. The small uncertainties stated lead to inconsistencies within the NIST results [9]. Since NIST does not state a single reference value for each sample, a direct comparison of reference values is not possible. However, the values determined here usually agree with those obtained by NIST with the same method, with the exception of DLS. Good agreement of NIST-TEM and PTB-TSEM measurements, not only with respect to the mean diameters but also considering the size distribution, has been shown [17]. In the case of SAXS, another independent study has been conducted by Bienert *et al* [43]. Within the scope of the expanded uncertainties, the measurement results agree with the SAXS measurements of PTB and NIST as well as with the comparison reference value determined here.

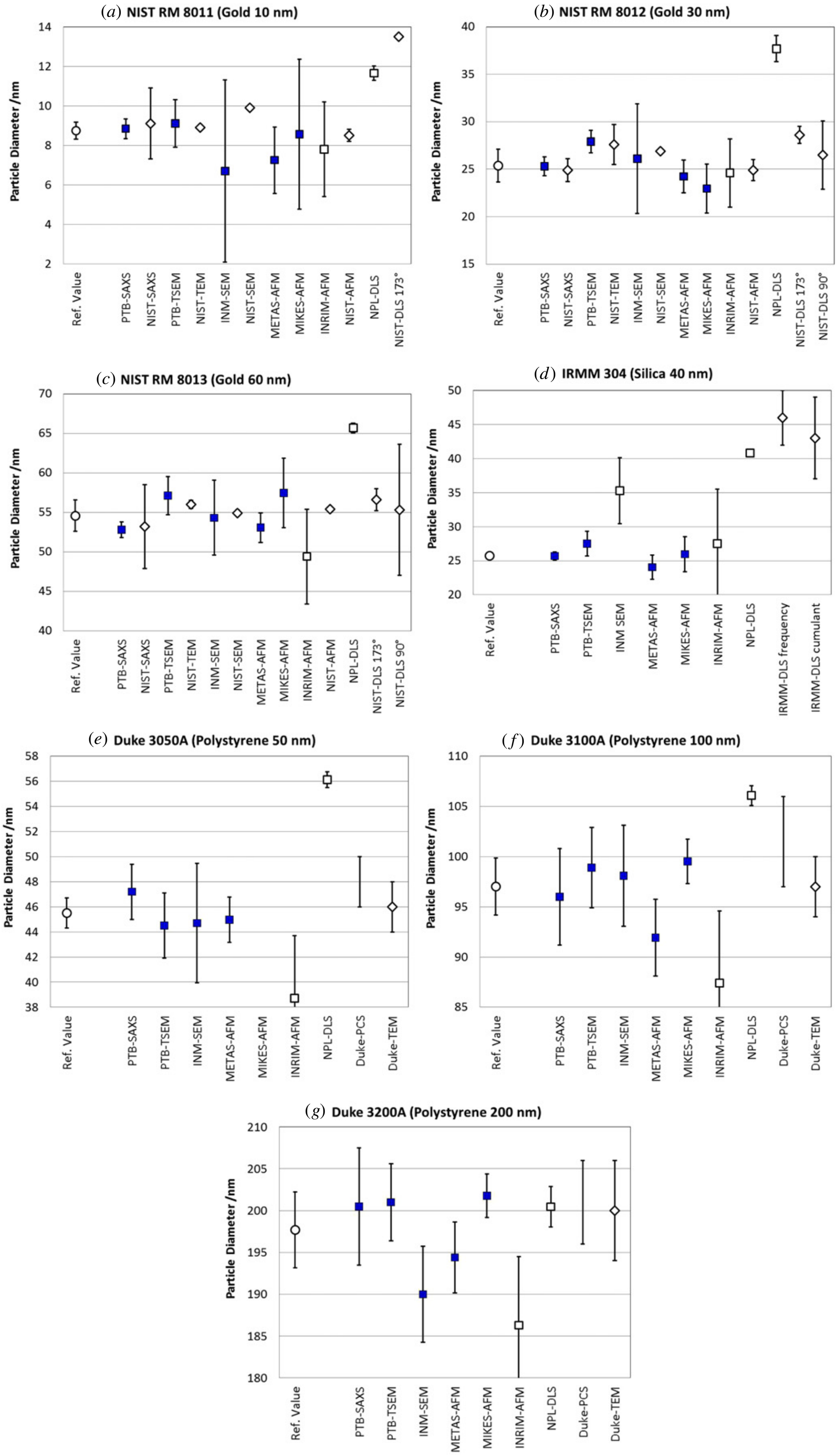

Figure 10. Graphical representation of the measurement results (squares), together with the comparison reference value (circle) and the particle sizes stated by the suppliers (diamonds). Measurement results not included in the calculation of the reference values have a white marker face. If no error bars are visible, the stated uncertainty is smaller than the dimension of the symbol. No marker for PCS indicates value range. Error bars indicate 95% confidence interval based on the stated uncertainties.

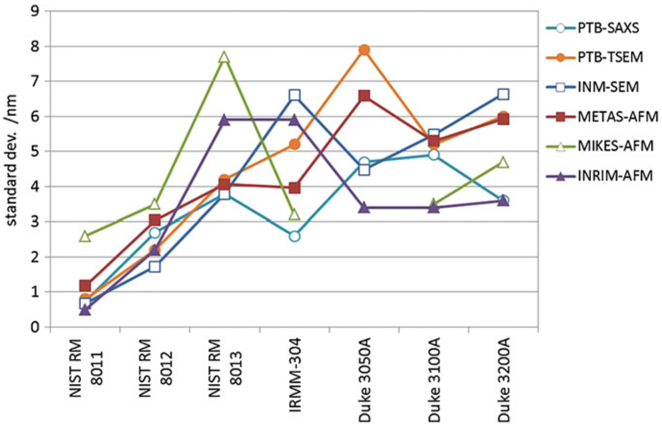

Figure 11. Standard deviations of the measured particle diameters.

For the IRMM silica sample, all measurement results agree with the exception of the SEM result which is a clear outlier. After its removal, the remaining four contributions to the reference value are consistent without the need to add an unknown uncertainty. Interestingly, the hydrodynamic values (between 43 and 46 nm) stated by IRMM [10] are far from the comparison reference value of 25.7 nm determined here. IRMM also conducted non-traceable TEM and AFM studies [44] which gave mean diameters of 24.7 nm for TEM and 28.4 nm for AFM and which are thus closer to the comparison reference value. Using imaging techniques the non-normal shape of the size distribution of the silica particles could be revealed. A slight bimodal distribution with a minor mode some nm smaller than the main mode was noticed with AFM, TSEM [18] and SEM, demonstrating an advantage they share compared to ensemble techniques. It is also present in the TEM measurements of the manufacturer [44].

For the Duke polystyrene particles, the Duke certified mean diameter, which is based on TEM measurements traceable to NIST certified microspheres, is consistent with the comparison reference value. This also holds for the range that is stated by Duke for the hydrodynamic diameter obtained with photon correlation spectroscopy (PCS). This study shows that the 50 nm polystyrene particles displayed a rather broad and irregular size distribution whereas the 100 and 200 nm particles have a much narrower distribution.

Figure 11 compiles the reported values for the standard deviation of the particle diameters which reflect mainly the width of the particle size distributions. Standard deviations for Duke 3100A agree within 1 nm except for two AFM measurements which reported slightly smaller values. The number of particles used to calculate the standard deviation was from 19 to several thousands. NPL reported the repeatability of the mean of a number of DLS measurements. These values are considerably smaller and are not included in figure 11. The sample with the narrowest absolute size distribution was NIST RM 8011 which probably has a Gaussian distribution. This also holds for the other gold samples. The sample with the smallest coefficient of variation (i.e. the standard deviation relative to the mean value) was Duke 3200A.

7. Conclusions

This particle size comparison among six European NMIs provided valuable results. It was probably the first nanoparticle comparison where all measurements are fully independent and directly traceable to the SI unit ‘metre’. The used particles are made from three different materials and have sizes in the range from 10 to 200 nm.

The five fundamentally different measurement methods (AFM, DLS, SAXS, SEM and TSEM), some working in air, others in vacuum or in liquid, showed, with the exception of DLS, no significant systematic differences.

The chosen method for the reference value estimation provides good consistency for most measurements. All comparison reference values with their uncertainties are valid and the set of particles given to each participant has gained a high additional value by this comparison. Additionally, the here determined unknown uncertainty contributions allow us to estimate the magnitude of not yet known influences.

The combined standard uncertainties of the reference values are smaller than 1.4 nm for particles with nominal sizes up to 100 nm and below 1.5% for the larger particles. The examined samples are still commercially available, although the latex samples may be from a different batch. Thus researchers from different fields may benefit from the thorough characterization and the precisely determined mean size. However, the use of these reference values for other samples of the same type is not recommended. Reliable samples need of course individual calibrations, preferably by an NMI.

Future work should attempt to clarify the unknown uncertainty contributions and the DLS method should be better understood in order to provide the same measurand as the other methods.

Acknowledgment

This work was supported by the EURAMET joint research project ‘Traceable measurement of nanoparticle size’ funded from the European Union’s Seventh Framework Programme, ERA-NET Plus, under Grant Agreement no 217257.

References

[1] Henson A 2009 Implementing the metrology European research area—iMERA *Publishable Final Activity Report* 6th framework programme of the European Commission

[2] Roadmap RM1—Micro and nano 2006 www.technology-roadmaps.eu (requires a free registration)

[3] Mulholland G W, Bryner N P and Croarkin C 1999 Measurement of the 100 nm NIST SRM 1963 by differential mobility analysis *Aerosol Sci. Technol.* **31** 39–55

[4] Germer T A, Mulholland G W, Kim J H and Ehrman S H 2002 Measurement of the 100 nm NIST SRM® 1963 by laser surface light scattering *Proc. SPIE* **4779** 60–71

[5] Jung K Y *et al* 2002 Measurement of 100-nm polystyrene sphere by transmission electron microscope *Powder Technol.* **126** 255–65

[6] Ehara K, Takahata K and Koike M 2006 Absolute mass and size measurement of monodisperse particles using a modified Millikan’s method: part II—application of electro-gravitational aerosol balance to polystyrene latex

particles of 100 nm to 1 μm in average diameter *Aerosol Sci. Technol.* **40** 521–35

[7] Wang C Y, Pan S P, Peng G S and Tsai J H 2005 A comparison study on the measurement of nanoparticles *Proc. SPIE* **5879** 323–8

[8] Wang C Y, Fu W E, Lin H L and Peng G S 2007 Preliminary study on nanoparticle sizes under the APEC technology cooperative framework *Meas. Sci. Technol.* **18** 487–95

[9] SRM 8011–8013, NIST, Standard Reference Materials, Gaithersburg, MD, United States www.nist.gov/srm

[10] IRMM-304, European Commission, Joint Research Centre, Institute for Reference Materials and Measurements, Geel, Belgium https://irmm.jrc.ec.europa.eu

[11] 3060A, 3100A and 3300A, Microgenics Corporation (Thermo Scientific), Fremont, CA, United States www.thermoscientific.com

[12] Beckhoff B, Gottwald A, Klein R, Krumrey M, Müller R, Richter M, Scholze F, Thornagel R and Ulm G 2009 A quarter-century of metrology using synchrotron radiation by PTB in Berlin *Phys. Status Solidi* B **246** 1415–34

[13] Gleber G, Cibik L, Haas S, Hoell S, Müller P and Krumrey M 2010 Traceable size determination of PMMA nanoparticles based on small angle x-ray scattering (SAXS) *J. Phys. Conf. Ser.* **247** 012027

[14] Krumrey M, Gleber G, Scholze F and Wernecke J 2011 Synchrotron radiation-based x-ray reflection and scattering techniques for dimensional nanometrology *Meas. Sci. Technol.* **22** 094032

[15] Kohlbrecher J 2009 SASfit, PSI Switzerland http://kur.web.psi.ch/sans1/SANSSoft/sasfit.html

[16] BIPM, IEC, IFCC, ILAC, ISO, IUPAC, IUPAP and OIML 2008 *Guide to the Expression of Uncertainty in Measurement* JCGM 100:2008, GUM 1995 with minor corrections, www.bipm.org/utils/common/documents/jcgm/JCGM_100_2008_E.pdf

[17] Klein T, Buhr E and Frase C G 2012 TSEM: a review of scanning electron microscopy in transmission mode and its applications *Advances in Imaging and Electron Physics* vol 171 ed P Hawkes (New York: Elsevier) pp 297–356

[18] Klein T, Buhr E, Johnsen K-P and Frase C G 2011 Traceable measurement of nanoparticle size using a scanning electron microscope in transmission mode (TSEM) *Meas. Sci. Technol.* **22** 094002

[19] Buhr E, Senftleben N, Klein T, Bergmann D, Gnieser D, Frase C G and Bosse H 2009 Characterization of nanoparticles by scanning electron microscopy in transmission mode *Meas. Sci. Technol.* **20** 084025

[20] Buhr E, Michaelis W, Diener A and Mirande W 2007 Multi-wavelength VIS/UV optical diffractometer for high-accuracy calibration of nano-scale pitch standards *Meas. Sci. Technol.* **18** 667–74

[21] Sadowski T E, Broadbridge C C and Daponte J 2007 Comparison of common segmentation techniques applied to transmission electron microscopy images *Mater. Res. Soc. Symp. Proc.* **982** 25–30

[22] Johnsen K P, Frase C G, Bosse H and Gnieser D 2010 SEM image modelling using the modular Monte Carlo model *Proc. SPIE* **7638** 76381O

[23] ASTM 2003 Standard practice for calibrating the magnification of a scanning electron microscope ASTM E 766-98

[24] Meli F, Thalmann R and Blattner P 1999 High precision pitch calibration of gratings using laser diffractometry *Proc. 1st Int. Conf. on Precision Engineering and Nanotechnology (Bremen)* ed P McKeown *et al* vol 2 pp 252–5

[25] Meli F 2000 Particle diameter calibration by means of a metrology AFM *Proc. 1st Euspen Topical Conf. on Fabrication and Metrology in Nanotechnology (Copenhagen)* ed L DeChiffre and K Carneiro vol 1 pp 45–51

[26] Meli F 2005 Lateral and vertical diameter measurements on polymer particles with a metrology AFM *Nanoscale Calibration Standards and Methods* ed G Wilkening and L Koenders (Weinheim: Wiley) ISBN 3-527-40502-X pp 361–74

[27] SPIP—Scanning probe image processor, Image Metrology A/S, Lyngsø Alle 3A, 2970 Hørsholm, Denmark www.imagemet.com

[28] Garnaes J 2011 Diameter measurements of polystyrene particles with atomic force microscopy *Meas. Sci. Technol.* **22** 094001

[29] Korpelainen V and Lassila A 2007 Calibration of a commercial AFM: traceability for a coordinate system *Meas. Sci. Technol.* **18** 395–403

[30] Korpelainen V, Iho A, Seppä J and Lassila A 2009 High accuracy laser diffractometer: angle-scale traceability by error separation method with a grating *Meas. Sci. Technol.* **20** 084020

[31] Korpelainen V, Seppä J and Lassila A 2010 Design and characterization of MIKES metrological atomic force microscope *Precis. Eng.* **34** 735–44

[32] Lassila A *et al* 2011 Design and performance of an advanced metrology building for MIKES *Measurement* **44** 399–425

[33] Stock R S and Ray W H 1987 Measuring particle-size distribution of latex-particles using dynamic light-scattering *ACS Symp. Ser.* **332** 105–14

[34] Koppel D E 1972 Analysis of macromolecular polydispersity in intensity correlation spectroscopy: the method of cumulants *J. Chem. Phys.* **57** 4814

[35] Granqvist C G and Buhrman R A 1976 Ultrafine metal particles *J. Appl. Phys.* **47** 2200–19

[36] Thomas J C 1987 The determination of log normal particle size distributions by dynamic light scattering *J. Colloid Interface Sci.* **117** 187–92

[37] International Standards Organisation, Geneva Particle size analysis—dynamic light scattering (DLS) ISO Standard 22412:2008

[38] Takahashi K, Kato H, Saito T, Matsuyama S and Kinugasa S 2008 Precise measurement of the size of nanoparticles by dynamic light scattering with uncertainty analysis *Part. Part. Syst. Charact.* **25** 31–8

[39] Birge R T 1932 The calculation of errors by the method of least squares *Phys. Rev.* **40** 207–27

[40] Kacker R, Datla R and Parr A 2002 Combined result and associated uncertainty from interlaboratory evaluations based on the ISO guide *Metrologia* **39** 279–93

[41] Boyd R D, Pichaimuthu S K and Cuenat A 2011 New approach to inter-technique comparisons for nanoparticle size measurements using atomic force microscopy, nanoparticle tracking analysis and dynamic light scattering *Colloids Surf.* A **387** 35–42

[42] Levenson M, Banks D, Eberhardt K, Gill L, Guthrie W, Liu H, Vangel M G, Yen J H and Zhang N F 2000 An approach to combining results from multiple methods motivated by the ISO GUM *J. Res. Natl Inst. Stand. Technol.* **105** 571–80

[43] Bienert R, Emmerling F and Thünemann A F 2009 The size distribution of 'gold standard' nanoparticles *Anal. Bioanal. Chem.* **395** 1651–60

[44] Couteau O, Charoud-Got J, Rauscher H, Franchini F, Rossi F, Kestens V, Franks K and Roebben G 2010 A colloidal silica reference material for nanoparticle sizing by means of dynamic light scattering and centrifugal liquid sedimentation *Part. Part. Syst. Charact.* **27** 112–24